

https://dspace.org/

Coemulsified AlginateEudragit Nanoparticles Potential Carriers for Localized and Timedefined Release of Tenofovir in the Female Genital Tract

Funanani Takalani; Pradeep Kumar; Pierre Kondiah; Yahya Choonara

SPRINGER
https://hdl.handle.net/10539/40880
WOS

Downloaded from a DSpace repository. https://dspace.org/

AAPS PharmSciTech (2024) 25:15
https://doi.org/10.1208/s12249-023-02723-4

RESEARCH ARTICLE

Co-emulsified Alginate-Eudragit Nanoparticles: Potential Carriers for Localized and Time-defined Release of Tenofovir in the Female Genital Tract

Funanani Takalani[1] · Pradeep Kumar[1] · Pierre P. D. Kondiah[1] · Yahya E. Choonara[1]

Received: 23 September 2023 / Accepted: 5 December 2023 / Published online: 10 January 2024
© The Author(s) 2024

Abstract
This research aimed to explore the possibilities of Eudragit S100 (ES100) and sodium alginate as carriers for tenofovir disoproxil fumarate (TDF) in the female genital tract. Alginate and alginate-ES100 nanoparticles were prepared using the ionic gelation and emulsion/gelation complexation method, respectively. The nanocarriers were tested using morphological, physicochemical, *in vitro* drug release, and cytotoxicity analyses. In SEM and TEM images, the presence of spherical and uniformly distributed nanoparticles was revealed. The FTIR spectrum showed that alginate and calcium chloride interacted due to ionic bonds linking divalent calcium ions and the -COO- of alginate groups. Alginate and ES100 interacted via the ester C=O amide stretching. The results obtained from XRD and DSC, on the other hand, revealed a favorable interaction between sodium alginate and ES100 polymers, as evidenced by the crystallization peaks observed. Under experimental design analysis and optimization, overall size distribution profiles ranged from 134.9 to 228.0 nm, while zeta potential results showed stable nanoparticles (−17.8 to −38.4 MV). The optimal formulation exhibited a maximum cumulative *in vitro* release of 72% (pH 4.2) up to 96 h. The cytotoxicity tests revealed the safety of TDF-loaded nanoparticles on vaginal epithelial cells at concentrations of 0.025 mg/mL, 0.5 mg/mL, and 1 mg/mL for 72 h. These results indicated that alginate-ES100 nanoparticles have the potential to preserve and sustain the release of the TDF drug in the FGT. The future goal is to develop a low-dose non-toxic microbicide that can be administered long term in the vagina to cater to both pregnant and non-pregnant HIV patients.

Keywords female genital tract · human immunodeficiency virus 1 · nanoparticles · sodium alginate · tenofovir disoproxil fumarate

Introduction

The female genital tract (FGT) possesses numerous characteristics in the mucosal immune system that render it suitable for the systemic dissemination of the human immunodeficiency virus (HIV-1) [1]. Nonetheless, nanotechnology for HIV-1 therapy has been cited as a technique capable of overcoming obstacles against HIV, thereby offering hope for HIV-1 care [2, 3]. Hence, nanomedicine-based therapies have been developed to facilitate the treatment of HIV-1 [4]. The primary objective is to formulate nanoparticles that can serve as carriers for delivering medications to precisely designated sites within the human body. Examples of these nanoparticles include polymeric nanoparticles, micelles, lipid nanoparticles, liposomes, and emulsions, which are further delineated in greater detail elsewhere [5].

Nanoparticles offer significant assurance in resolving issues related to various biological barriers, as they protect drugs from degradation through their controlled and sustained delivery [6]. Nanoparticles have also been used to improve the oral absorption of drugs that are accompanied by limited permeation, low solubility, and chemical instability [7]. One of these drugs is the Tenofovir Disoproxil Fumarate (TDF) HIV drug. The TDF is categorized within a group of antiretroviral medications known as nucleotide reverse transcriptase inhibitors (NRTIs). It is a preferred

✉ Yahya E. Choonara
yahya.choonara@wits.ac.za

[1] Wits Advanced Drug Delivery Platform Research Unit, Department of Pharmacy and Pharmacology, School of Therapeutic Sciences, Faculty of Health Sciences, University of the Witwatersrand, Johannesburg, 7 York Road, Parktown 2193, South Africa

first-line regimen for both men and women [8]. Several studies have incorporated TDF into nanoparticles for antiviral protection [7, 9–11]. However, although this drug effectively prevents mother-to-child transmission and manages pre-exposure prophylaxis (PrEP) and hepatitis B, there is a rising concern regarding its long-term effects [8].

On the contrary, it has been reported that Eudragit S100 (ES100) may prolong the release of drugs in various parts of the body. However, only a few studies have used this polymer in the FGT. Eudragits have been shown to regulate drug release due to their dissolution and osmotic release patterns [12]. Furthermore, the burst effect, which is associated with accelerated drug release and therapeutic effects, is diminished due to the insoluble nature of ES100 under acidic pH conditions [13, 14]. Given this information, we found it intriguing to develop alginate-ES100 nanoparticles for the extended release of TDF drug in the FGT. The selection of these polymers was influenced by their toxicological information, as both have been reported to be non-toxic [15, 16]. ES100 is a non-biodegradable polyanionic copolymer of methacrylic acid and methyl methacrylate [16–18]. Eudragit polymers are generally recommended for developing novel drug delivery systems and fabricating sustained-release formulations [12, 17, 19]. Furthermore, ES100 has been demonstrated to possess a high degree of adhesion, moderate swelling, and superior mechanical properties [18]. In contrast to ES100, sodium alginate is a biodegradable natural polymer that is readily accessible and renowned for its low-cost production [15, 20, 21]. This hydrogel-based polymer is suited for the delivery of hydrophilic drugs, such as TDF, owing to its capacity to absorb substantial quantities of water while maintaining its structure [21]. Lastly, its mucoadhesive and immunogenic properties make it an outstanding drug-delivery polysaccharide. This research aimed to develop co-emulsified alginate-ES100 nanoparticles and assess their potential as carriers for the TDF antiretroviral drug in the FGT. The rationale for conducting this study is that the current oral dose of the TDF drug on the market is 300 mg, which is associated with elevated kidney toxicity and changes in bone density if taken for a prolonged period [22, 23]. Our research therefore sought to develop a system that would have a lower TDF dose (based on its water-soluble nature), reduced toxicology, and a longer release of the TDF drug. Moreover, our primary objective was to devise a formulation that would be subsequently incorporated into a microbicide that would be administered topically in the vagina to both pregnant and non-pregnant women to prevent HIV infection. In this case, the utilization of alginate nanoparticles was the best choice, as they have been reported to improve the bioavailability of drugs [21]. Together with ES100, they are both non-toxic and recommended for controlled drug delivery, as mentioned before. Various techniques including SEM, TEM, *in vitro* drug release, FTIR, DSC, and XRD were employed, followed by the execution of the experimental design (Box-Behnken) and the execution of a cytotoxicity MTT assay for further analysis and optimization.

Materials and Methods

Materials

The ES100, sodium alginate (low molecular weight), calcium chloride, methanol, dimethyl sulfoxide (DMSO), MTT assay, and the constituents of the simulated vaginal fluid (SVF) such as glucose, sodium chloride, lactic acid, potassium hydroxide, glacial acetic acid, urea, calcium hydroxide, and glycerin were obtained from Sigma–Aldrich (St. Louis, Missouri, USA). After that, the TDF drug was purchased from Leap Chem (Easey Com BLDG 253-261, Hong Kong). Life Bioscience (Oakleigh, VIC, Australia) provided vaginal cells (VK2), penicillin/streptomycin, and fetal bovine serum (FBS). All the supplementary reagents or chemicals utilized were of superior quality.

Preparation of Alginate and Alginate-ES100 TDF-loaded Nanoparticles

Alginate Nanoparticles

The ionic gelation technique [24] was employed to prepare several trial formulations (Supplementary Table I) to evaluate the formation of alginate nanoparticles. To summarize and utilize the most successful trial formulation (Supplementary Fig. 1 (F3)), 90 mg of sodium alginate and 60 mg of TDF were dissolved in 15 mL of water, resulting in a 0.6% alginate solution. On the contrary, a concentration of 25 mg of $CaCl_2$ was dissolved in 45 mL of water to form a 0.06% $CaCl_2$ solution. Subsequently, the alginate solution was introduced in droplets into the $CaCl_2$ solution under the influence of the magnetic stirrer at 1.5 RPM. After an hour of stirring, the particles were collected by centrifugation for 10 min at 12100 RPM. In the end, the suspension was frozen at −80°C and lyophilized at −37°C for a duration of 12 h.

Alginate-ES100 Nanoparticles

As previously discussed, F3 (shown in Supplementary Fig. 1) was selected as the optimal alginate trial formulation, which resulted in the subsequent synthesis of alginate-ES100 nanoparticles. This was accomplished using the emulsion/gelation complexation method [21], which is the most widely used and recent manufacturing technique for alginate-based nanoparticulate delivery systems [21]. The preparation of the alginate-in-oil (w/o) emulsion is the first

step in this technique, followed by the gelation of the alginate emulsion droplets with a covalent or ionic cross-linker. This method was most effective for mixing alginate and the ES100 polymer, which is partially soluble in water. Hence, we first dispersed it in methanol before combining it with alginate. Thus, different ratios (1:2, 1:1, 2:1, and 1:1.4) for Alginate: ES100 were employed, as presented in Supplementary Table II. Using a 1:1 ratio as an example (F6, Supplementary information), 90 mg of ES100 and 60 mg of TDF were mixed in 5-mL methanol under the magnetic stirrer to form a 2% ES100 solution. Afterward, 90 mg of alginate was thawed separately in 15 mL to form a 0.6% alginate solution. For 5 min, these two solutions were mixed under a magnetic stirrer, then further sonicated for another 5 min to create an emulsion. After this, the mixture was added dropwise to a 0.06% $CaCl_2$ solution, under the same magnetic stirrer at a stirring speed of 1.5 RPM. The composite was subjected to stirring for an hour under the fume hood to evaporate methanol, and nanoparticles were collected by centrifugation for 10 min at 12100 RPM. Finally, the suspension was frozen overnight and then lyophilized at −37°C for 12 h. The same preparation steps were followed for TDF-free nanoparticles, except that the TDF drug was not added.

Characterization of Nanoparticles

Morphological Analyses

The SEM (JEOL JSM, Tokyo) was used at an acceleration voltage of 15 keV to view the outward morphology of nanoparticles. Before visualization, the powder nanoparticles were placed on standard pin stubs and coated with gold palladium. Furthermore, TEM was employed to observe nanoparticles by utilizing high-energy electron beams. In this instance, a droplet of the suspension was fixed onto a carbon grid and subjected to analysis at a voltage of 120 keV using JEOL 1200 EX.

Nanoparticles Size, Zeta Potential, and Polydispersity Index (PDI)

The Malvern Zetasizer Nano ZS instrument, manufactured in Worcestershire, UK, was utilized. Here, 2 mL of the freshly prepared formulation was mixed with 3 mL of purified water for a total of 5 mL. The mixture was then sonicated for 2 min at a probe temperature of 20°C with a 20% amplitude and pulsation (50 s of sonication with a 10-s pause). Afterward, the nanoparticles were analyzed for size, zeta potential, and PDI using the dynamic light scattering technique at an angle of 175°. Capillary cell cuvettes were employed, and intensity was recorded at 25°C. Measurements were taken in threefold increments.

Fourier Transform Infrared Spectroscopy (FTIR)

By observing vibrational frequency bands, we determined the structural variations of the nanoparticles formed. This was done to confirm the backbone structure and integrity of the main effective groups of the TDF drug, alginate, and ES100 polymers during nanoparticle formation. Samples were positioned on a diamond crystal and processed by a PerkinElmer Spectrum 2000 ATR-FTIR (PerkinElmer 100, Llantrisant, Wales, UK). The FTIR conditions were as indicated: 24 scans at a 4 cm^{-1} resolution and a wavelength number ranging from 4000 to 650 cm^{-1}.

X-ray Diffraction (XRD)

X-ray wave interference was observed to further analyze nanoparticles and characterize the stage categories involved. First, the spectra were recorded on a MiniFlex 600 benchtop diffractometer (Rigaku, Japan) using a copper anode (CuKα) at 40 kV radiation and 15 mA. Then, a scan of 2θ was conducted at a speed of ten degrees per minute, between 10 and 90 degrees. This was followed by diffraction analyses, which allowed for the observation of the nanoparticles' crystallinity degree.

Differential Scanning Calorimetry (DSC)

The thermodynamic compatibility between alginate, ES100, and the TDF drug was investigated using the DSC technique (Mettler Toledo, STARe System, Swchwerzenback, ZH, Switzerland). This was accomplished by evaluating their transition from glass to liquid and melting conditions. In this study, samples ranging from 3 to 10 mg were weighed, sealed in aluminum vessels, and subjected to warming at a temperature range of 10 to 350°C. The melting rate was ten degrees per minute in a nitrogen gas atmosphere. Then, the DSC graphs were presented as the flow of heat *versus* temperature.

Determining the Entrapment Efficiency (EE%) and Drug Loading Capacity (DL%) of Nanoparticles

As shown below and reported by Schafroth and co-workers (2011), Eqs. (1) and (2) were used to calculate the EE% and DL% of TDF-loaded nanoparticles, respectively. Thus, the absorbance of the TDF was calculated using the ultraviolet-visible spectrophotometer (Specord 40 UV-vis Spectrophotometer, Analytic Jena AG, Jena, Germany) at 265 nm.

$$EE\% = \frac{drug\ within\ nanoparticle}{Initial\ amount\ of\ drug} X100 \quad (1)$$

$$DL\% = \frac{amount\ of\ drug\ in\ nanoparticles}{amount\ of\ nanoparticle} X100 \quad (2)$$

In Vitro Release of TDF-loaded Nanoparticles

The cumulative release profiles of TDF from TDF-loaded nanoparticles were determined by the dialysis bag diffusion method [25]. In this instance, the simulated vaginal fluid (SVF, pH 4.2) was utilized as the release medium to preserve sink conditions for TDF. Briefly, 10 mg of TDF-loaded nanoparticles and 2 mL of SVF buffer were introduced into dialysis bags with a relative molecular mass cutoff of 12 kDa. These were submerged in 50-mL SVF buffer and placed in an orbital shaker, where they were stirred at 25 RPM, with the temperature set at 37°C. Subsequently, at designated elapsed times (1 h, 3 h, 6 h, 9 h, 12 h, 24 h, 48 h, 72 h, and 96 h), 2 mL of the release buffer was withdrawn and promptly replaced with fresh release buffer. The amounts of TDF liberated from the samples were quantified at a wavelength of 265 using an ultraviolet-visible spectrophotometer, and the results were displayed as the cumulative release percentage of the drug over time. The standard curve equation for the TDF drug was $Y = 0.0192x$ ($R^2 = 0.9999$), as shown in Supplementary Fig. 2. All procedures were undertaken in triplicate alongside a blank control formulation.

Development of the Experimental Design

To ensure the quality, safety, and efficacy of the formulations developed, the experiment design was generated. The response surface methodology (RSM) design was particularly applicable in this study as it requires few experimental runs [26, 27]. Hence, a fractional factorial design composing three factors and three levels was generated using Minitab statistical software (MINITAB®, V15, Minitab, USA). The development of 15 formulations corresponding to 15 runs was conducted with a single center point. Then, the upper and lower actual values for critical input factors were determined (shown in Table I). In contrast, critical processing parameters such as temperature, volume, stirring speed, sizes of beakers, and sizes of stirrers were kept constant. The output critical responses, including drug release percentage (DR %), mean particle size (PS), zeta potential (ZP), and polydispersity index (PDI), were chosen for this design. Then, the results of these responses were incorporated into the quadratic polynomial equation as shown below:

$$Y = [Alginate].[Eudragit].[CaCl2].[Alginate] * [Alginate].[Eudragit] * [Eudragit].[CaCl2] * [CaCl2].[Alginate] * [Eudragit].[Alginate] * [CaCl2].[Eudragit] * [CaCl2] \quad (3)$$

Here, Y represents the measured responses, while Alginate, Eudragit, and CaCl2 are input factors. The models were validated by applying an analysis of variance (ANOVA) test. A probability of 0.05 was considered to be the significant level with $P < 0.05$, and $P > 0.1$ was deemed nonsignificant due to a lack of fit. Furthermore, regression analysis and coefficient of determination tests were conducted to evaluate the suitability of the models. Then, surface plots were employed to analyze the interactions among variables.

Table I Upper and Lower Actual Values for Input Critical Factors

Input variables	Lower values (mg)	Upper values (mg)
Alginate	90	130
ES100	90	180
$CaCl_2$	15	25

Optimization Using the Desirability Function

Based on the results obtained from the 15 formulations, the responses for PDI, mean particle size, and drug release % were further optimized following the desirability function approach [28]. Therefore, three formulations were processed using the approximate values, as depicted in Table II. These formulations were prepared following the same method described in the "Preparation of Alginate and Alginate-ES100 TDF-loaded Nanoparticles" section. In addition to this, methods used to characterize or analyze responses for size/PDI, EE%/DL%, and DR% were also the same as those explained in "Nanoparticles Size, Polydispersity Index (PDI), and Zeta Potential," "Determination of EE% and DL% of Nanoparticles," and "*In vitro* Release of TDF-loaded Nanoparticles" sections, respectively. All experiments were undertaken in triplicate.

Table II Desirability and Predicted Values for the Optimized Formulations

Solution	Alginate (mg)	Eudragit (mg)	$CaCl_2$ (mg)	PDI fit	PS (nm) fit	DR% fit	Composite desirability
1	117.879	123.636	19.8485	0.143019	147.245	0.757158	0.932483
2	126.266	106.368	18.9104	0.142274	155.351	0.742039	0.884029
3	113.042	144.517	19.2536	0.157497	150.104	0.754622	0.879090

Cell Culture and Cytotoxicity Studies

The MTT assay was selected to analyze the toxic effects of TDF-loaded nanoparticles, drug-free nanoparticles, and TDF on vaginal epithelial cells (VK2). Therefore, cells were grown and maintained as described by Zhang and co-workers [11]. To summarize, VK2 cells were cultured in DMEM/F12 media, enriched with 1% penicillin-streptomycin and 10% FBS, in 25-cm^2 culture flasks until they reached 80–90% confluence. Then, the cells were slid into a 96-well plate with 1×10^4 cells per well. Afterward, the plates were left to equilibrate for 24 h at 37°C to secure their attachment. Subsequently, the cells that were attached underwent treatment in pentaplicates ($n = 5$) with varying concentrations (0.025 mg/mL, 0.5 mg/mL, and 1 mg/mL) of TDF-loaded nanoparticles, drug-free nanoparticles, and TDF. An untreated medium was considered a positive control, whereas DMSO was considered a negative control. After the treatment, the well plates were left in the incubator for set time points, 24 h and 72 h. Then, 10 µL of MTT-media solution was poured into each well, and the plates were incubated for 4 h. After that, 100 µL of media was taken out, and 100 µL of the solubilizing agent was introduced. This was followed by further overnight incubation of the plates at 37°C to liquefy the formazan. Lastly, the multimodal microplate reader (Victor X3, manufactured by Perkin Elmer in Waltham, MA, USA) was employed to obtain the results at an absorbance of 570–690 nm.

Results and Discussion

Morphology of Alginate Nanoparticles as well as Alginate-ES100 Nanoparticles

SEM analysis demonstrated the existence of alginate nanoparticles, whereas both SEM and TEM results showed the existence of alginate-ES100 nanoparticles (Fig. 1). The findings regarding alginate nanoparticles were in agreement with those reported by Thomas and co-workers in 2020 and 2021 [29, 30] and by Kumar and co-workers in 2014 and 2017 [31, 32], indicating the difficulties encountered in forming proper spherical nanoparticles by the alginate polymer. As a result, we introduced the ES100 polymer into the alginate system, and as we expected, the results for this confirmed the formation of nanoparticles that were more defined in shape and smooth on the surface, as shown in Fig. 1. Similar outcomes have been reported for nanoparticle systems that have been incorporated with ES100, thereby confirming that ES100 is indeed capable of forming spherical nanoparticles. Some of these reports have been authored by Yoo et al. in 2011, Sharma et al. in 2011, Anwer et al. in 2017, Zhang et al. in 2011, and Saraf et al. in 2019 [11, 13, 14, 33, 34].

Nanoparticle size, Polydispersity Index (PDI), and Zeta Potential

The mean particle size, the PDI, and the zeta potential are critical parameters for drug delivery systems [20]. Alginate-ES100 formulations had average sizes between 134.9 and 228.0 nm (Table III), which could be explained by the encapsulation with a hydrophilic compound [33]. Moreover, the lower PDI values in the range of 0.129–0.363 indicate the physical stability of the systems and the uniform dispersion of particles [13, 35]. The zeta potential results indicated that nanoparticles with high negative charges were stable. System stability is indicated by zeta potentials around +/−30 MV. [35, 36]. As per the finding of Subudhi et al. (2015), elevated negative potentials result in an electric repulsion that prevents the degradation of particles. Hence, in contrast to nanoparticles that possess a positive charge, which bind to the cell membranes through electrostatic interaction with the negatively charged membrane, the mucosa's cellular uptake of negatively charged particles primarily pertains to the formation of loose assimilation of the particles, which encircle the surface of the plasma membrane. Secondly, it pertains to the production of nanoparticle clusters [20]. In this study, negative zeta potentials were expected since both alginate and ES100 are anionic. Irvin-choy and colleagues (2020) [4] reported that size and surface charge have the potential to influence the circulation of nanoparticles in living organisms. Hence, zeta potential is regarded as a significant component that reveals the formation of nanoparticles because it indicates the net charges obtained by particles in a particular medium [37]. Furthermore, negatively charged nanoparticles are more suitable for vaginal application, whereas larger sizes (>100 nm) could be utilized to target the placenta, since maternal blood is directly linked to the syncytial membrane [4, 38].

Fourier Transform Infrared Spectroscopy

The FTIR spectra of neat polymers (Fig. 2) revealed results like those previously reported. Thus, the infrared spectrum of ES100 revealed vibrational frequency bands at 1450 cm^{-1}, which correspond to the presence of the -CH_3 bend, and at 1275–1000 cm^{-1}, which are attributed to C=O amide stretching from esterified carboxylic groups and C-F bonds [34, 39, 40]. The alginate spectrum, on the other hand, revealed absorption peaks at 1616 cm^{-1} and 1418 cm^{-1}, which correspond to COO- asymmetric and symmetric stretching vibrations, respectively [15, 41, 42]. Furthermore, the bands at 1092 and 1032 correspond to the C-O and CO-C groups in the mannuronic and guluronic units, respectively. The vibration bands of alginate and ES100 carboxylic groups suggest that O-H exists in their structures at 3500–3000 cm^{-1} [25]. When the two polymers are

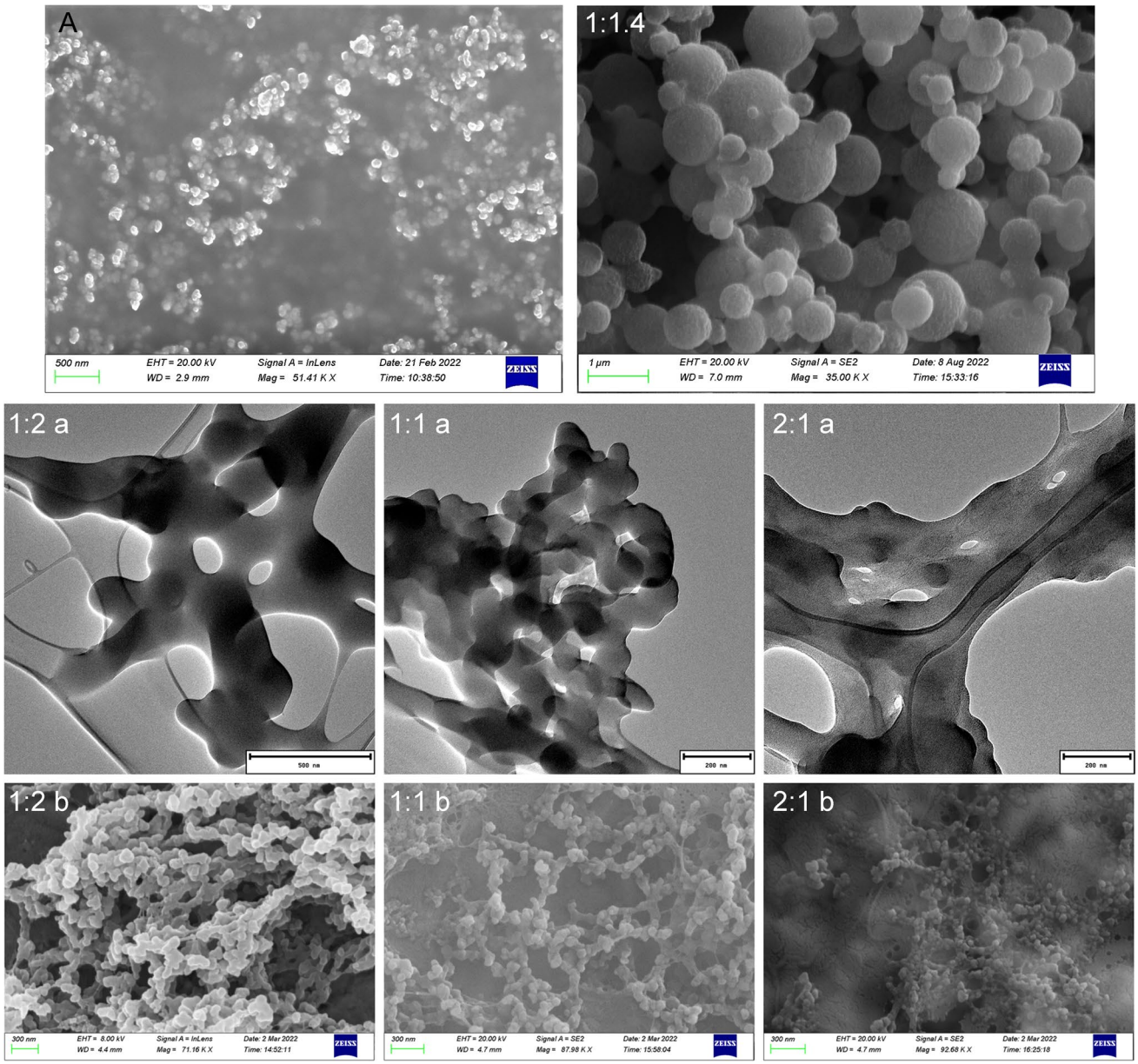

Fig. 1 **A** SEM image of alginate nanoparticles taken at a scale of 500 nm. Ratios 1:1.4, 1:2b, 1:1b, and 2:1b: SEM images of the TDF drug loaded into alginate-ES100 nanoparticles. Images were taken at a scale of 1 µm and 500 nm**.** Ratios 1:2a, 1:1a, and 2:1a: TEM images of the TDF drug loaded into alginate-ES100 nanoparticles. Images were taken at a scale of 500 nm (1:2a) and 200 nm (1:1a and 2:1a)

cross-linked (Alg-ES100), slight variations were observed at 1616–1603 cm^{-1} and 1418–1410 cm^{-1} in comparison to the alginate spectra alone. The reduction in wave numbers confirmed a firm indication of intermolecular interactions, potentially related to the development of ionic bonds in divalent calcium ions and the -COO- groups of alginates [30, 43]. In this context, the substitution of sodium ions with calcium ions in alginate blocks results in modifications in the atomic weight, charge density, and radius of cations. Upon the formation of nanoparticles, this creates a different setting around the carbonyl group [30, 43]. Altogether, calcium chloride and alginate polymer interacted via the asymmetric and symmetric alginate stretching of COO- [29]. Then, calcium alginate interacted with ES100 via the C=O ester bond to form a new strong anhydride bond at 1050–1040 cm^{-1}. A proposed mechanism for this interaction is depicted in Fig. 3. A shift in the carboxylate peak position from 1728 to 1560 cm^{-1} has been observed during the ionization process of ES100. This phenomenon is attributed to the anti-symmetrical COO- vibration [40, 44]. Nonetheless, there was no discernible shift in the spectrum of Alg-TDF-ES100 pertaining to this band, indicating that no recent

Table III Box-Behnken Experimental Design: Formulation Variables and Responses of Alginate-ES100 Nanoparticles (All Analyses were Undertaken in Triplicate)

Run order	Alginate (mg)	ES100 (mg)	$CaCl_2$ (mg)	Maximum cumulative release % at 96 hrs	Mean particle size (nm)	Zeta potential (MV)	PDI
F1	110	135	20	75%	146.9 ± 0.69	−29.9 ± 0.79	0.153 ± 0.02
F2	110	135	20	75%	147.5 ± 0.70	−30.7 ± 0.81	0.145 ± 0.02
F3	110	180	25	60%	157.7 ± 4.15	−25.1 ± 1.29	0.206 ± 0.01
F4	90	90	20	50%	228.0 ± 5.34	−17.8 ± 0.31	0.254 ± 0.04
F5	110	90	25	53%	150.7 ± 3.61	−30.8 ± 5.70	0.184 ± 0.02
F6	110	180	15	64%	178.8 ± 2.75	−25.1 ± 6.86	0.261 ± 0.01
F7	90	135	25	74%	182.6 ± 3.12	−32.4 ± 2.69	0.245 ± 0.01
F8	130	135	25	77%	179.7 ± 6.38	−31.9 ± 0.93	0.252 ± 0.01
F9	130	135	15	73%	179.5 ± 4.36	−35.5 ± 1.91	0.239 ± 0.01
F10	110	90	15	53%	149.9 ± 1,34	−38.4 ± 5.39	0.154 ± 0.01
F11	110	135	20	75%	148.7 ± 0.73	−28.2 ± 0.77	0.154 ± 0.02
F12	130	90	20	73%	157.9 ± 1.03	−38.4 ± 1.85	0.129 ± 0.02
F13	130	180	20	68%	185.8 ± 1.21	−32.6 ± 0.57	0.216 ± 0.01
F14	90	135	15	72%	194.6 ± 4.04	−35.2 ± 4.81	0.211 ± 0.02
F15	90	180	20	62%	198.9 ± 4,72	−29.5 ± 0.66	0.248 ± 0.01

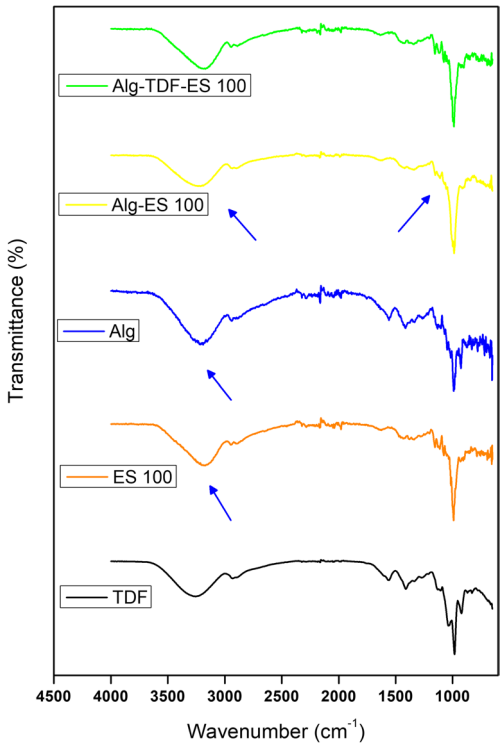

Fig. 2 FTIR spectra of the TDF drug, ES100, alginate (Alg), Alg + TDF, unloaded (Alg-ES100), and TDF-loaded nanoparticles (Alg-TDF-ES100)

chemical bond was established either after the formulations production or during lyophilization. These results confirm the dispersion of TDF in the polymers and demonstrate an effective interaction between alginate and ES100 polymers. This interaction possesses characteristics that may have resulted in the entrapment of TDF within alginate-ES100 nanoparticles. Furthermore, the fusion of the polymers with the drug (Alg-TDF-ES100) showed peaks similar to those of Alg-ES100, which confirms that no interaction occurred between the polymers and the drug [45].

X-ray Diffraction

XRD was used to evaluate the crystalline structures of raw polymers and nanoparticles. Figure 4 shows the X-ray diffraction graphs of ES100, sodium alginate, and the TDF drug, as well as drug-free nanoparticles (Alginate-ES100) and TDF-loaded nanoparticles. This data indicated that alginate formed a semi-crystalline pattern, consistent with previous reports [46–49]. Furthermore, the alginate diffraction peaks at $2\theta = 14.5°$ and 22.0° correspond to the humidified atomic arrangement formed by hydrogen covalent bonding [48]. On the contrary, ES100 is a nebulous powder devoid of crystalline structure, as exemplified by the diffraction pattern. These results agree with those reported by Hu et al., 2012, Sharma et al., 2012, Yusuf et al., 2021, and Ding et al., 2020 [34, 50–52]. The TDF drug powder is crystalline and shows clear, sharp peaks, unlike sodium alginate and ES100. According to El-Sheikh and co-workers (2018) [53], sharp, clear peaks are associated with the high purity of the systems [53]. Interestingly, sodium alginate and the ES100 polymer interacted well, as shown by the green graph of drug-free nanoparticles. This confirms nanoparticle formation. The interaction between these polymers could be attributed to the functional groups of the ES100 polymer,

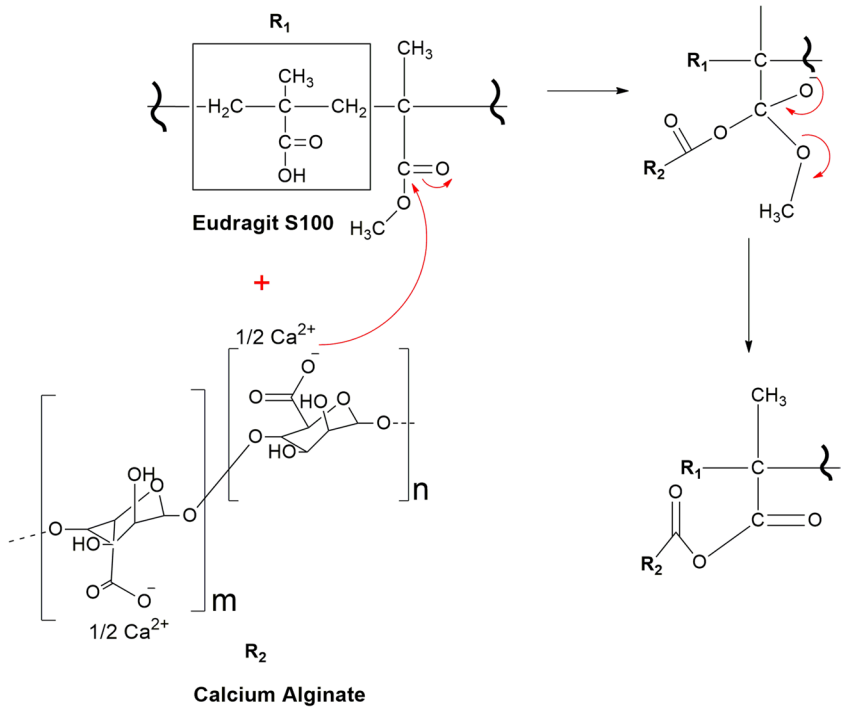

Fig. 3 A proposed mechanism of calcium alginate and eudragit S100 interaction

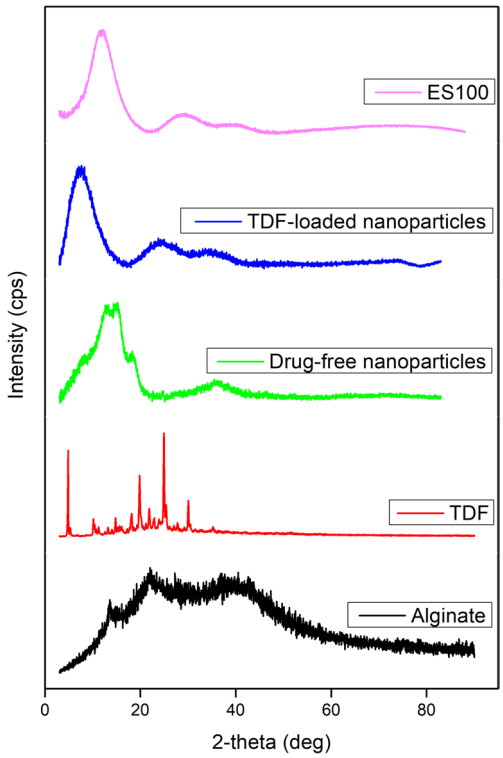

Fig. 4 X-ray diffraction patterns of alginate, TDF drug, ES100, drug free (Alg-ES100), and TDF-loaded nanoparticles (Alg-TDF-ES100)

as similarities between the ES100, drug-free nanoparticles, and TDF-loaded nanoparticles graphs depict. Moreover, the sharp, clear peaks of the TDF drug that disappeared in TDF-loaded nanoparticles indicated that encapsulation had occurred [14]. In this invention, the TDF molecule was converted into a nebulous state to coincide with alginate and ES100 polymers.

Differential Scanning Calorimetry

The DSC instrument is used to ascertain the melting behavior of polymers and the glass transition temperature [42]. It is dependent on the sample's thermal capacity as a function of temperature [54]. For the sodium alginate polymer, endothermic and exothermic peaks were observed at 123.57°C and 235.02°C, respectively, as shown in Fig. 5. As per the findings of Chawla et al. (2012) and Siddaramaiah et al. (2008), the endothermic peak is attributed to the evaporation of water and the carboxylate segment of the polymer [55, 56], whereas the exothermic peak may be attributed to the diaxial and diequatorial links of the polymer segments [55]. The sodium alginate contains three polymer sections, one with varying units of sugar, the other with poly(β-D-mannopyranosyluronate), and the third with poly(α-L-guluopyranosyluronate). Based on the diaxial and diequatorial links between these segments, sodium alginate displays a weakened and narrow melting pinnacle at 220°C [55]. Additionally, alginate is an amorphous polymer that does not crystallize due to its irregular or geometrical structure. This conclusion is in accordance with the publications of Soares et al. (2004) and El-Houssiny et al. (2016) [57, 58], wherein the authors reported that the thermal degradation of sodium alginate involves three distinct stages.

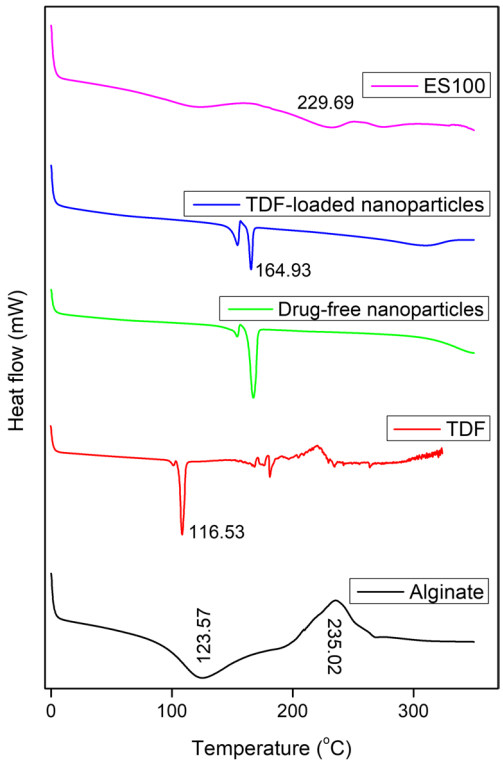

Fig. 5 DSC thermograms of alginate, TDF drug, ES100, drug free (Alg-ES100), and TDF-loaded nanoparticles (Alg-TDF-ES100)

The first step is an endothermic peak indicating the dehydration process and glass transition temperature at around 80 °C. Then, an endothermic peak nearing 200°C, which is associated with the melting point, followed by an exothermic peak at around 240°C [46, 55, 57, 58]. In addition to the thermogram peaks for sodium alginate, endothermic peaks were observed for the unbound TDF, ES100, and nanoparticles loaded with TDF at 116.53°C, 229.69°C, and 164.93°C, respectively, indicating their melting points and crystallization. The TDF and ES100 peaks are in agreement with previous findings [7, 59, 60]. The overall results indicated that the endothermic peak of TDF was lowered in TDF-loaded nanoparticles. These findings suggest thermodynamic compatibility between alginate, ES100, and the TDF drug, as the shifts of the endothermic and exothermic peaks correspond to links connecting drugs and polymers [54, 58].

Determination of EE% and DL% of Nanoparticles

The results regarding entrapment efficiencies and drug loading capacities of the 15 formulations are presented in Supplementary Fig. 3. Entrapment efficiency refers to the percentage of TDF entrapped in the nanoparticles relative to the overall sum of TDF introduced during the production of the system [61]. This is the primary factor affecting drug release and the overall efficacy of the formulation process. Our results confirmed that most of the drug was entrapped, ranging from 74% (F5) to 88% (F9). High entrapment efficiency was achieved by keeping the drug concentration and stirring speed constant while varying the alginate, calcium chloride, and ES100 concentrations. Cautela et al. (2018) and Pokharkar et al. (2015) have previously published comparable findings indicating a high EE% for the TDF drug encapsulated into nanoparticles. Drug loading, on the other hand, is described as the mass of TDF available in nanoparticles (100 mg) [32]. It is therefore dependent on the initial drug/polymer ratio [62]. As depicted in Supplementary Fig. 1, the results obtained for drug loading capacities ranged from 13% (F13) to 20% (F4). Based on the drug release results in the "Differential scanning calorimetry" section, these results confirmed successful loading, as the drug loading must ensure adequate release from the nanosystem [63]. Furthermore, Shen and colleagues (2017) reported that drug loading is considered high when it exceeds 10% [64], as evidenced by our findings for all formulations. Overall, the formulations of alginate-ES100 nanoparticles demonstrated the ability to preserve the TDF drug, leading to a prolonged release.

In Vitro Release of TDF-loaded Nanoparticles

Graphs A–E (Fig. 6) show that half of the TDF was released from alginate-ES100 nanoparticles within the initial 12 h, whereas the remaining concentration was sustained for 96 h. Table III shows that the maximum cumulative release of F1–F15 was achieved at 96 h. Increasing concentrations of alginate and eudragit resulted in an increased release of the drug. These outcomes are consistent with those reported by Zhang and co-workers (2011) [11], who found that drug release increased with increasing concentrations of the ES100 polymer. The outcome was expected, as eudragits are known to regulate drug release due to their dissolution and osmotic release patterns [12]. Furthermore, ES100 exhibits insoluble properties in acidic pH conditions, thereby reducing the burst effect, which is associated with accelerated drug release and therapeutic effects [13, 14]. On the contrary, calcium alginate undergoes a solvable transformation in the presence of sodium salts, thereby facilitating the extension of the encapsulated TDF release [32]. Our results demonstrated an improved cumulative release compared to previous reports on the release of the TDF drug [7, 9, 11].

Experimental Design Analysis

As depicted in Table III, the model responses were determined based on the results of the 15 experimental runs. The adequacy of these models was then verified by applying several tests, such as ANOVA, regression analysis, and coefficient of determination, while surface plots were used

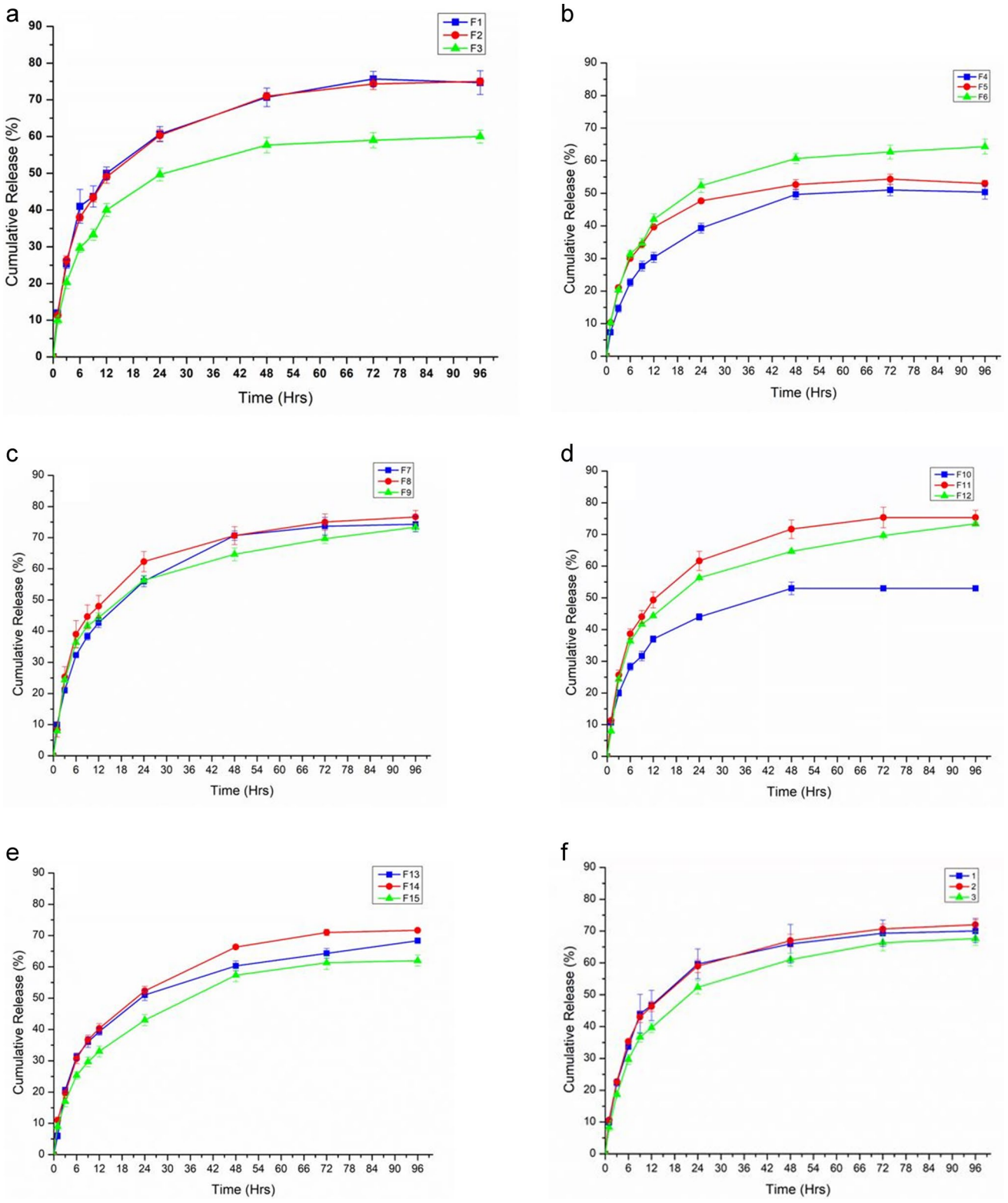

Fig. 6 Cumulative *in vitro* release of the experimental design formulations [**a**–**e** (F1–F15)] and the optimized formulations [**f** (1–3)] in simulated vaginal fluid (SVF) at pH 4.2. The release was sustained for up to 96 h

to analyze interactions between variables. The results of the ANOVA test (Supplementary Tables III, IV, V, and VI) revealed that the probability values for the F-statistics of drug release % and mean particle size responses were both 0.004, which implies that these models were significant ($P < 0.05$) and that they fitted well in the quadratic model. PDI (0.088) and zeta potential (0.403) responses were insignificant, which could be attributed to the fact that no statistical variation was detected for these models. However, the lack of fit p values was all significant ($P < 0.1$), except for the DR% model, which did not show any lack of fit. Therefore, the values of the lack of fit for PDI, mean particle size, and zeta potential models were 0.016, 0.006, and 0.042, respectively.

These models lacked prediction efficiency, as a lack of fit with high nonsignificant values ($P > 0.1$) is desired for a quadratic model [26, 65]. Under the coefficient of determination, the R^2 values were high and close to 1 (see Supplementary Tables III, IV, V, and VI). This indicates that the mathematical model was adequate, and the optimization was appropriately validated [27, 66]. Furthermore, the difference between R^2 and R^2-adjusted values is expected to be lower than 0.2, which was the case for drug release percentage and mean particle size models. This is an indication that the models adopted were significant [67]. However, the difference between the R^2 and the R^2-adjusted values for PDI and zeta potential was higher than 0.2. It is important to note that these results are consistent with those of the ANOVA test above. Figure 7a, on the other hand, displays linear regression models (normal probability plots), non-linear regression models (*versus* fits), histogram graphs, and *versus* order for all responses.

Linear regression models revealed normal distribution analysis as evidenced by the straight lines and minor deviations from linear distribution [27, 68, 69]. In contrast, non-linear regression models displayed randomness, with the standard error of the regression (S) for drug release %, mean particle size, PDI, and zeta potential being 0.0397762, 10.4184, 0.0314322, and 5.04154, respectively (Supplementary Tables III, IV, V, and VI). The dispersion of these responses is unbiased and forms constant variance as the small S values present it. The presence of smaller S values indicates that points are situated closer to the fitted line. Histogram plots confirmed the uniform distribution of the results, as shown by the bell shapes evenly distributed around zero. Moreover, the *versus* order patterns displayed the overall results of the 15 formulations for each response. The formulas for multiple linear regression or quadratic polynomial equations for all responses are shown below (Eqs. (4)–(7)). For the DR% model, the coefficient values are as follows: Alginate is −0,0046, eudragit is 0.02472, and CaCl2 is 0.0545. For the PS model, alginate is −21,89, eudragit is −2,48, and CaCl2 is 2,48. Similarly, for the PDI model, alginate is −0,03066, eudragit is −0,00214, and CaCl2 is −0.0484. Lastly, for the ZP model, alginate is 0,26, eudragit is -0,591, and CaCl2 is 5,03. These responses had intercepts of −1,375; 1532; 2,463; and −52, respectively.

$$\begin{aligned} DR\% = {} & -1,375 - 0,0046[Alginate] + 0,02472[Eudragit] \\ & + 0,0545[CaCl2] + 0,000059[Alginate] * [Alginate] \\ & - 0,000070[Eudragit] * [Eudragit] - 0,001350[CaCl2] \\ & * [CaCl2] - 0,000047[Alginate] * [Eudragit] \end{aligned} \tag{4}$$

$$\begin{aligned} PS(nm) = {} & 1532 - 21,89[Alginate] - 2,48[Eudragit] + 2,48[CaCl2] \\ & + 0,0869[Alginate] * [Alginate] + 0,00491[Eudragit] \\ & * [Eudragit] + 0,01583[Alginate] * [Eudragit] \\ & - 0,0243[Eudragit] * [CaCl2] \end{aligned} \tag{5}$$

$$\begin{aligned} PDI = {} & 2,463 - 0,03066[Alginate] - 0,00214[Eudragit] - 0,0484[CaCl2] \\ & + 0,000119[Alginate] * [Alginate] + 0,000006[Eudragit] * [Eudragit] \\ & + 0,001542[CaCl2] * [CaCl2] + 0,000027[Alginate] * [Eudragit] \\ & - 0,000094[Eudragit] * [CaCl2] \end{aligned} \tag{6}$$

$$\begin{aligned} ZP = {} & -52 + 0,26[Alginate] - 0,591[Eudragit] + 5,03[CaCl2] \\ & - 0,00484[Alginate] * [Alginate] + 0,00097[Eudragit] \\ & * [Eudragit] - 0,089[CaCl2] * [CaCl2] \\ & + 0,00486[Alginate] * [Eudragit] - 0,0084[Eudragit] * [CaCl2] \end{aligned} \tag{7}$$

In addition to the aforementioned analysis, response surface plots were employed to examine additional interactions among process variables. The effects of polymers and the cross-linking agent on DR%, PS, PDI, and ZP measurements were evaluated, as depicted in Fig. 7b. This was presented as a function of alginate and eudragit, alginate and $CaCl_2$, and eudragit and $CaCl_2$. The percentages of drug release exhibited an increase with the increase in concentrations of both alginate and eudragit at any $CaCl_2$ concentration. However, particle size, zeta potential, and PDI increased with decreasing alginate concentrations and increasing concentrations of eudragit. It is noteworthy that as the concentrations of eudragit increase, the concentrations of $CaCl_2$ for particle size and PDI decrease. Overall, the results suggested that alginate and eudragit play an important role in sustaining the release, stabilizing, dispersing, and controlling the particle size of the systems. These outcomes are in accordance with the findings presented in Table II and the "Differential scanning calorimetry" section.

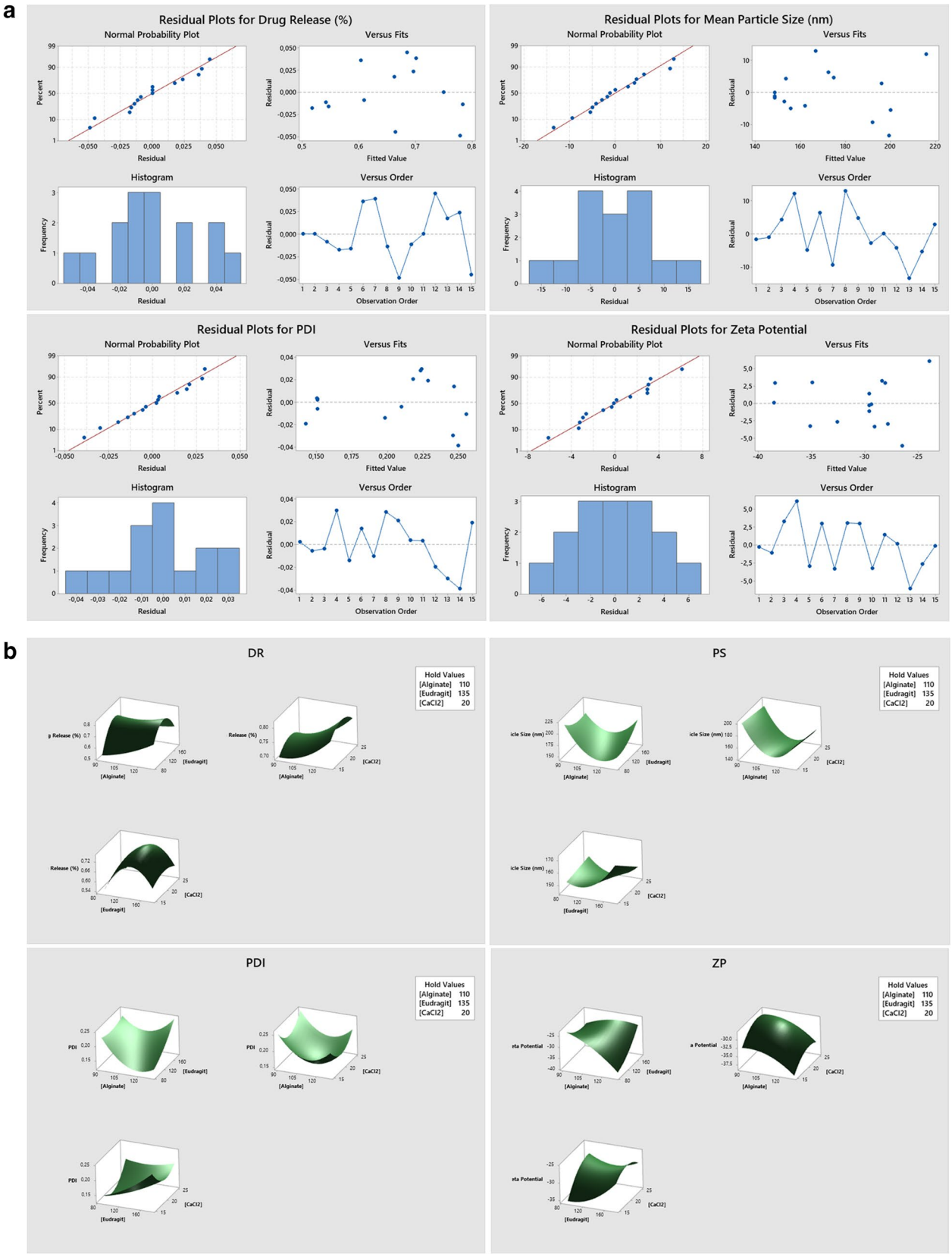

Fig. 7 **a** Residual plots and **b** 3-D response surface plots for drug release, mean particle size, poly dispersity index, and zeta potential

Optimization Using the Desirability Function

As shown in Table II, the desirability indexes for the three optimized formulations (01, 02, and 03) were 0.932482, 0.884029, and 0.879090, respectively, considered within the acceptable range [70]. The experimentally derived PDI values for these formulations were 0.251 ± 0.03, 0.220 ± 0.04, and 0.197 ± 0.02, respectively, whereas mean particle size values were 134.9 ± 2.34, 155.9 ± 1.55, and 183.6 ± 2.17. We found it necessary to conduct an analysis for both size and PDI, as they go hand in hand. PDI shows how narrow the particle size distribution is. If the value is less than 0.1, it means that the distribution is minimal. In drug delivery, a PDI of 0.3 or less is good because it proves that the particles are all the same size [71]. It is generally observed that the more homogeneous the particle size, the more stable the properties of polymers and small particles are. The utilization of stable properties can yield significant advantages in their respective fields. Consequently, it is important to achieve a homogeneous size of nanoparticles with a small PDI. The maximum cumulative release values were 70%, 72%, and 68%, respectively, as depicted in Fig. 6f. These results are consistent with the predicted values in Table II. However, the results for 02 closely match the approximated values, followed by 01 and 03. This confirms the reliability of the experimental design approach in predicting the most suitable formulation suitable for TDF release from alginate-ES100 nanoparticles. Furthermore, the maximum cumulative release for these formulations was 96 h, which aligns with the maximum cumulative release of F1–F15 in the "Differential scanning calorimetry" section. On the contrary, the EE percentage of all formulations 01, 02, and 03 was 84%, whereas the DL percentage of 01 and 02 was 17% and the DL percentage of 03 was 16%. It is worth noting that the higher concentration of eudragit in formulation 03 resulted in a DL% that was lower than that of formulations 01 and 02. This supports the notion we discussed in the "X-ray Diffraction" section that higher concentrations of alginate/eudragit polymers result in lower DL%. Moreover, in contrast to the EE% range (74–88%) of the 15 formulations, the optimized formulations also exhibited EE% within this range, indicating that the majority of the drug was entrapped.

Cytotoxicity Assessment of Alginate-ES100 TDF-loaded Nanoparticles

The TDF drug has been reported to be tolerated for a short period by HIV patients, but if used for a long time, it can result in renal and bone cytotoxicity [23]. In this research, our primary objective was to sustain the release of TDF by incorporating it into non-toxic polymers such as alginate and ES100. Hence, we conducted an MTT cytotoxicity assay utilizing TDF-loaded nanoparticles, drug-free nanoparticles, and TDF on VK2 cells. A vaginal microbicide is considered safe if it does not damage the vaginal epithelium, cause distress which would decrease patient compliance, and require low doses for therapy [72, 73]. Moreover, it is imperative that the safety profiles for topical strategies to prevent HIV infection justify their implementation on the vaginal ecology and mucosal integrity [11]. Our data revealed that nanoparticles loaded with TDF did not exhibit any cytotoxic effects on VK2 cells for a duration of 24–72 h (as depicted in Fig. 8) at concentrations of 0.025 mg/mL, 0.5 mg/mL, and 1 mg/mL. The viability exhibited a significant increase with the increase in nanoparticle concentration, reaching its utmost level at 1 mg/mL. Thus, cell viability remained above 90% at this concentration for up to 72 h, and no serious decrement was noticed compared to the positive control. These reactions are in agreement with those reported by Zhang et al. in 2013 [73], who conducted cytotoxicity studies on tenofovir incorporated into eudragit S-100 sodium salt microspheres at a concentration of 1 mg/mL on VK2 cells. Furthermore, the findings presented by Meng et al. in 2017 and Yoo et al. in 2010 have demonstrated that alginate and eudragit S-100 polymers play a significant role in sustaining high cell viability on VK2 cells. Moreover, no significant reduction was observed for alginate and eudragit particles at various concentrations, up to 1 mg/mL [33, 72]. In general, it appears that the cell viability of the pure TDF drug is lower than that of the TDF-loaded nanoparticles. This indicates that the toxicity level of our designed formulation is superior to that of the TDF drug alone, rendering alginate and ES100 polymers suitable carriers for the TDF drug with the potential for sustained delivery in the FGT.

Clinical Significance of the Study

After the conception process, the fertilized egg divides into cells, resulting in the formation of a zygote. This embeds itself in the uterine wall, triggering the growth of the fetus and placenta [4]. As gestation progresses, the chorionic villus begins to separate into various layers. Initially, extravillous trophoblasts penetrate and obstruct maternal spiral arteries, thereby preventing the flow of blood to the developing fetus. This provides a hypoxic condition for the fetus, which protects it from early damage caused by oxidative stress. Meanwhile, the uterine glands provide nutrients to the fetus [4]. Secondly, villous trophoblasts produce syncytiotrophoblasts, a site where P-gp is highly expressed in the placenta. The syncytiotrophoblasts directly interact with the maternal blood to form a strong barrier that unites the circulatory systems of the mother and child. Hence, at the commencement of the second trimester, the plug that encloses the maternal spiral arteries during differentiation is released, thereby allowing blood from the maternal region to flow into the placenta and fetus [4]. When taken together, the fetus has

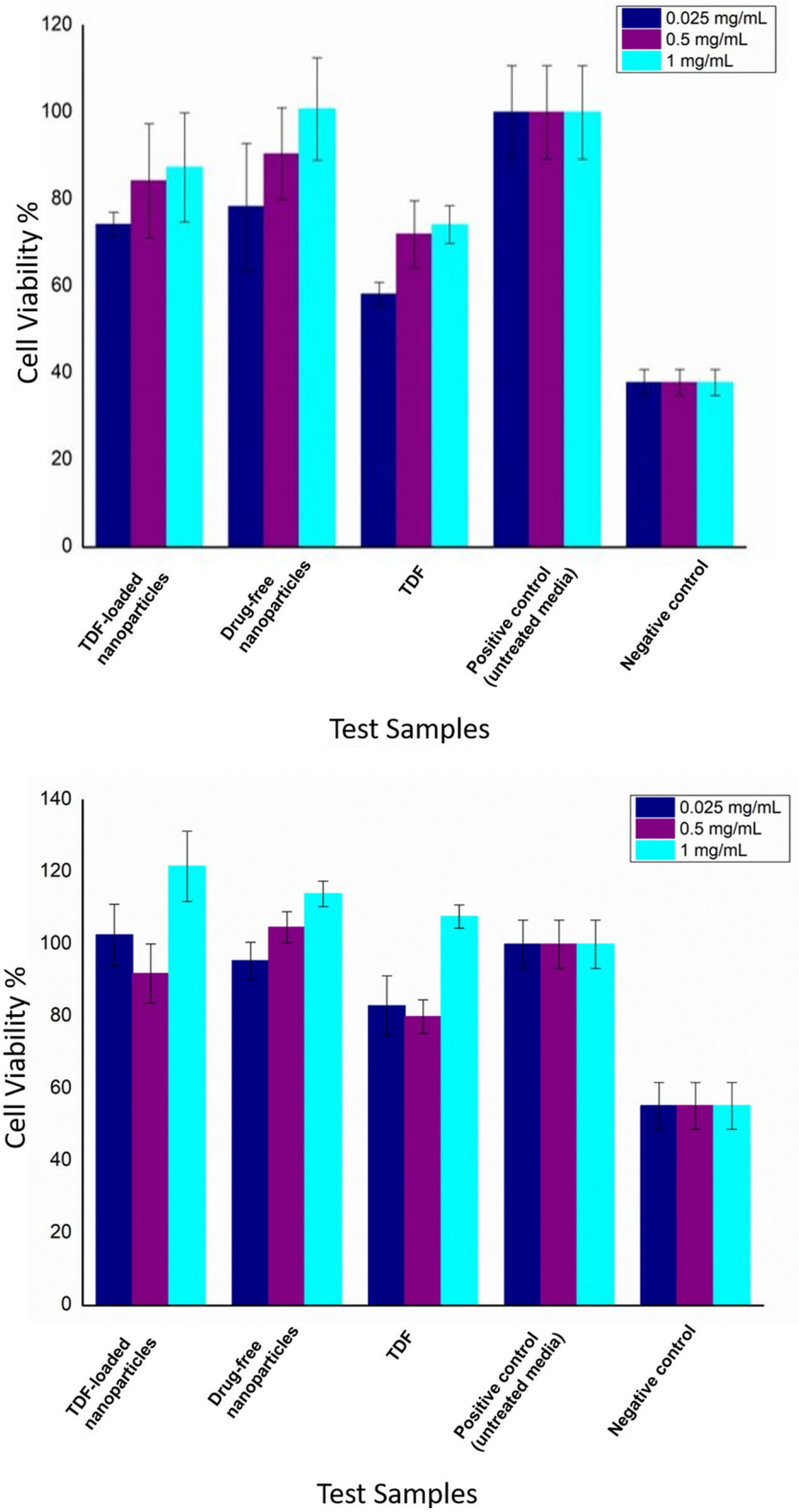

Fig. 8 Cell viability for TDF-loaded nanoparticles, drug-free nanoparticles, and TDF at 24 h and 72 h

a greater capacity to be exposed to maternal drugs nearing birth term. It is noteworthy that the transport of drugs or other molecules from the maternal circulation to the placenta and fetus can be altered. Although, to attain this objective, nanomedicine must be constructed in a manner that enables them to overcome multiple biological obstacles to reach the fetus. The implementation of targeted treatments, with the aim of preventing transfer via the placenta or facilitating

transport to treat the fetus, would yield significant advantages, resulting in optimal care for both the mother and the fetus. We are aiming to develop a topical delivery system that can be administered vaginally to pregnant women during the first trimester to increase the transfer of the TDF drug from maternal to fetal circulation.

Conclusion

According to our understanding, this study describes the successful synthesis of the TDF antiretroviral drug loaded into alginate-ES100 nanoparticles. The particle size, encapsulation efficiency, and zeta potential were established to be suitable for the FGT environment. The drug release profiles showed a high release, sustained for 96 h at pH 4.2, corresponding to the FGT pH. Following the statistical ANOVA test, the overall optimization results demonstrated that the mathematical model was adequate. This was exemplified by the R^2 values, as well as the S and low F-statistics *P* values, which were found to be significant and within the desired ranges for nearly all models. The exception was the lack of fit *P* values for all models, which were not as high as anticipated to fit well in the quadratic model. However, the system revealed significant interactions between dependent and independent variables, as shown in response surface plots. The cytotoxicity evaluation demonstrated the safety of alginate-ES100 TDF-loaded nanoparticles in the female genital tract. Hence, it can be inferred that alginate-ES100 nanoparticles possess the capability to effectively preserve and sustain TDF release in the FGT. However, it would be imperative to conduct a thorough investigation of the therapeutic implications of this system *in vivo* to ensure the viability of nanomedicine in the future. The long-term objective is to develop a low-dose non-toxic microbicide that can be administered long term in the vagina to cater to both pregnant and non-pregnant HIV patients.

Supplementary Information The online version contains supplementary material available at https://doi.org/10.1208/s12249-023-02723-4.

Author Contribution **Funanani Takalani:** experimentation; methodology; writing – original draft

Pradeep Kumar: conceptualization; supervision; funding acquisition; writing – review and editing

Pierre Kondiah: protocol methods

Yahya Choonara: conceptualization; supervision; funding acquisition; project administration; writing – review and editing

Funding Open access funding provided by University of the Witwatersrand. This work was funded by the National Research Foundation (NRF) SARChI Grant and the South African Medical Research Council (SAMRC) under Bongani Mayosi National Health Scholarship (BMNHSP), Research Capacity Development (RCD) Grant.

Data Availability Data is available on request from the authors.

Declarations

Conflict of interest The authors declare no competing interests.

Open Access This article is licensed under a Creative Commons Attribution 4.0 International License, which permits use, sharing, adaptation, distribution and reproduction in any medium or format, as long as you give appropriate credit to the original author(s) and the source, provide a link to the Creative Commons licence, and indicate if changes were made. The images or other third party material in this article are included in the article's Creative Commons licence, unless indicated otherwise in a credit line to the material. If material is not included in the article's Creative Commons licence and your intended use is not permitted by statutory regulation or exceeds the permitted use, you will need to obtain permission directly from the copyright holder. To view a copy of this licence, visit http://creativecommons.org/licenses/by/4.0/.

References

1. Reis Machado J, Da Silva MV, Cavellani CL, Antônia Dos Reis M, Monteiro MLGDR, Teixeira VDPA, et al. Mucosal immunity in the female genital tract, HIV/AIDS. Biomed Res. Int. Hindawi Limited; 2014.
2. Corsi F, Sorrentino L, Mazzucchelli S, Truffi M, Capetti A, Rizzardini G, et al. Antiretroviral therapy through barriers: a prominent role for nanotechnology in HIV-1 eradication from sanctuaries. 2016;4:328–39.
3. Das MK, Chakraborty T. Progress in brain delivery of Anti-HIV drugs. J Appl Pharm Sci. 2015;5:154–64.
4. Irvin-Choy NS, Nelson KM, Gleghorn JP, Day ES. Design of nanomaterials for applications in maternal/fetal medicine. J. Mater. Chem. B. Royal Society of Chem; 2020. p. 6548–61.
5. Takalani F, Kumar P, Kondiah PPD, Choonara YE, Pillay V. Lipid–drug conjugates and associated carrier strategies for enhanced antiretroviral drug delivery. Pharm. Dev. Technol. Taylor and Francis Ltd; 2020. p. 267–80.
6. Beloqui A, Solinís MÁ, Gascón AR, Del Pozo-Rodríguez A, Des Rieux A, Préat V. Mechanism of transport of saquinavir-loaded nanostructured lipid carriers across the intestinal barrier. J Control Release. 2013;166:115–23.
7. Shailender J, Ravi PR, Saha P, Dalvi A, Myneni S. Tenofovir disoproxil fumarate loaded PLGA nanoparticles for enhanced oral absorption: effect of experimental variables and in vitro, ex vivo and in vivo evaluation. Colloids Surfaces B Biointerfaces. 2017;158:610–9.
8. Olojede SO, Lawal SK, Dare A, Naidu ECS, Rennie CO, Azu OO. Evaluation of tenofovir disoproxil fumarate loaded silver nanoparticle on testicular morphology in experimental type-2 diabetic rats. Artif Cells, Nanomedicine Biotechnol. 2022;50:71–80.
9. Cautela MP, Moshe H, Sosnik A, Sarmento B, das Neves J. Composite films for vaginal delivery of tenofovir disoproxil fumarate and emtricitabine. Eur J Pharm Biopharm. 2019;138:3–10.
10. Sarma A, Das MK. Formulation by design (FbD) approach to develop tenofovir disoproxil fumarate loaded nanostructured lipid carriers (NLCs) for the aptness of nose to brain delivery. J Drug Deliv Ther. 2019;9:148–59.
11. Zhang T, Sturgis TF, Youan BBC. PH-responsive nanoparticles releasing tenofovir intended for the prevention of HIV transmission. Eur J Pharm Biopharm. 2011;79:526–36.
12. An overview of multifaceted significance of eudragit polymers in drug delivery systems.

13. Saraf A, Dubey N, Dubey N, Sharma M. Box Behnken design based development of curcumin loaded eudragit s100 nanoparticles for site-specific delivery in colon cancer. Res J Pharm Technol. 2019;12:3672–8.
14. Anwer MK, Al-Shdefat R, Ezzeldin E, Alshahrani SM, Alshetaili AS, Iqbal M. Preparation, evaluation and bioavailability studies of Eudragit coated PLGA nanoparticles for sustained release of eluxadoline for the treatment of irritable bowel syndrome. Front Pharmacol. 2017;8.
15. Joshy KS, George A, Jose J, Kalarikkal N, Pothen LA, Thomas S. Novel dendritic structure of alginate hybrid nanoparticles for effective anti-viral drug delivery. Int J Biol Macromol. 2017;103:1265–75.
16. Thakral S, Thakral NK, Majumdar DK. Eudragit®: a technology evaluation. Expert Opin. Drug Deliv. 2013. p. 131–49.
17. Ansari F, Pourjafar H, Jodat V, Sahebi J, Ataei A. Effect of Eudragit S100 nanoparticles and alginate chitosan encapsulation on the viability of Lactobacillus acidophilus and Lactobacillus rhamnosus. AMB Express. 2017;7.
18. Cazorla-Luna R, Martín-Illana A, Notario-Pérez F, Miguel Bedoya L, Tamayo A, Ruiz-Caro R, et al. Vaginal polyelectrolyte layer-by-layer films based on chitosan derivatives and Eudragit® S100 for pH responsive release of tenofovir. Mar Drugs. 2020;18.
19. Sonje A, Chandra A. Comprehensive review on eudragit polymers. Int Res J Pharm. 2013;4:71–4.
20. Spadari C de C, de Bastiani FWM da S, Lopes LB, Ishida K. Alginate nanoparticles as non-toxic delivery system for miltefosine in the treatment of candidiasis and cryptococcosis. Int J Nanomedicine. 2019;14:5187–99.
21. Choukaife H, Doolaanea AA, Alfatama M. Alginate nanoformulation: influence of process and selected variables. Pharmaceuticals. MDPI AG; 2020. p. 1–35.
22. De Clercq E. Tenofovir alafenamide (TAF) as the successor of tenofovir disoproxil fumarate (TDF). Biochem Pharmacol. 2016;119:1–7.
23. Foster C, Lyall H, Olmscheid B, Pearce G, Zhang S, Gibb DM. Tenofovir disoproxil fumarate in pregnancy and prevention of mother-to-child transmission of HIV-1: is it time to move on from zidovudine? HIV Med. 2009. p. 397–406.
24. Zimet P, Mombrú ÁW, Faccio R, Brugnini G, Miraballes I, Rufo C, et al. Optimization and characterization of nisin-loaded alginate-chitosan nanoparticles with antimicrobial activity in lean beef. LWT. 2018;91:107–16.
25. Kianersi S, Solouk A, Saber-Samandari S, Keshel SH, Pasbakhsh P. Alginate nanoparticles as ocular drug delivery carriers. J Drug Deliv Sci Technol. 2021;66.
26. Regun Karmoker J, Hasan I, Ahmed N, Saifuddin M, Selim Reza M. Development and optimization of acyclovir loaded mucoadhesive microspheres by Box-Behnken design.
27. Aliemeke BNG, Oladeinde M. Box-Behnken design optimization of sand casting process parameters. Int J Eng Technol IJET. 2020;6:25–36.
28. Reis SDS, Quintanilha Junior VDS, Boto GDS, Da Silva TM, Macedo EV, Peregrino CA de F, et al. Use of Box–Behnken design for optimization of compounded medication: acyclovir capsules report. Drug Anal Res. 2021;5:59–67.
29. Thomas D, Mathew N, Nath MS. Starch modified alginate nanoparticles for drug delivery application. Int J Biol Macromol. 2021;173:277–84.
30. Thomas D, KurienThomas K, Latha MS. Preparation and evaluation of alginate nanoparticles prepared by green method for drug delivery applications. Int J Biol Macromol. 2020;154:888–95.
31. Kumar S, Bhanjana G, Sharma A, Sidhu MC, Dilbaghi N. Synthesis, characterization and on field evaluation of pesticide loaded sodium alginate nanoparticles. Carbohydr Polym. 2014;101:1061–7.
32. Kumar S, Bhanjana G, Verma RK, Dhingra D, Dilbaghi N, Kim KH. Metformin-loaded alginate nanoparticles as an effective antidiabetic agent for controlled drug release. J Pharm Pharmacol. 2017;69:143–50.
33. Yoo JW, Giri N, Lee CH. PH-sensitive Eudragit nanoparticles for mucosal drug delivery. Int J Pharm. 2011;403:262–7.
34. Sharma M, Sharma V, Panda AK, Majumdar DK. Development of enteric submicron particle formulation of papain for oral delivery. Int J Nanomedicine. 2011;6:2097–111.
35. Vlaia L, Coneac G, Muţ AM, Olariu I, Vlaia V, Anghel DF, et al. Topical biocompatible fluconazole-loaded microemulsions based on essential oils and sucrose esters: formulation design based on pseudo-ternary phase diagrams and physicochemical characterization. Processes. 2021;9:1–21.
36. Anicescu MC, Dinu-Pîrvu CE, Talianu MT, Ghica MV, Anuța V, Prisada RM, et al. Insights from a Box–Behnken optimization study of microemulsions with salicylic acid for acne therapy. Pharmaceutics. 2022;14.
37. Mujtaba MA, Alotaibi NM. Chitosan-sodium alginate nanoparticle as a promising approach for oral delivery of rosuvastatin calcium: formulation, optimization and in vitro characterization. J Pharm Res Int. 2020;50–6.
38. Menezes V, Malek A, A. Keelan J. Nanoparticulate drug delivery in pregnancy: placental passage and fetal exposure. Curr Pharm Biotechnol. 2012;12:731–42.
39. De Leo V, Di Gioia S, Milano F, Fini P, Comparelli R, Mancini E, et al. Eudragit s100 entrapped liposome for curcumin delivery: anti-oxidative effect in Caco-2 cells. Coatings. 2020;10.
40. Silva AE, Oliveira EE, Gomes MCS, Marcelino HR, Silva KCH, Souza BS, et al. Producing xylan/Eudragit® S100-based microparticles by chemical and physico-mechanical approaches as carriers for 5-aminosalicylic acid. J Microencapsul. 2013;30:787–95.
41. Derkach SR, Voron'ko NG, Sokolan NI, Kolotova DS, Kuchina YA. Interactions between gelatin and sodium alginate: UV and FTIR studies. J Dispers Sci Technol. 2020;41:690–8.
42. Jana S, Kumar Trivedi M, Tallapragada RM. Characterization of physicochemical and thermal properties of chitosan and sodium alginate after biofield treatment. Pharm Anal Acta. 2015;6.
43. Daemi H, Barikani M. Synthesis and characterization of calcium alginate nanoparticles, sodium homopolymannuronate salt and its calcium nanoparticles. Sci Iran. 2012;19:2023–8.
44. Raffin RP, Colomé LM, Pohlmann AR, Guterres SS. Preparation, characterization, and in vivo anti-ulcer evaluation of pantoprazole-loaded microparticles. Eur J Pharm Biopharm. 2006;63:198–204.
45. Mehta R, Chawla A, Sharma P, Pawar P. Formulation and in vitro evaluation of Eudragit S-100 coated naproxen matrix tablets for colon-targeted drug delivery system. J Adv Pharm Technol Res. 2013;4:31–41.
46. Nair RM, Bindhu B, L R V. A polymer blend from Gum Arabic and Sodium Alginate - preparation and characterization. Available from: https://doi.org/10.1007/s10965-020-02128-y
47. Eltaweil AS, Mamdouh IM, Abd El-Monaem EM, El-Subruiti GM. Highly efficient removal for methylene blue and Cu2+onto UiO-66 metal-organic framework/carboxylated graphene oxide-incorporated sodium alginate beads. ACS Omega. 2021;
48. Wang H, Chen X, Wen Y, Li D, Sun X, Liu Z, et al. A study on the correlation between the oxidation degree of oxidized sodium alginate on its degradability and gelation. Polymers (Basel). 2022;14.
49. Bhagyaraj S, Krupa I. Alginate-mediated synthesis of heteroshaped silver nanoparticles and their hydrogen peroxide sensing ability. Molecules. 2020;25.
50. Hu D, Liu L, Chen W, Li S, Zhao Y. A novel preparation method for 5-aminosalicylic acid loaded eudragit S100 nanoparticles. Int J Mol Sci. 2012;13:6454–68.

51. Yusuf H, Rahmawati RA, Rijal MAS, Isadiartuti D. Curcumin micelles entrapped in eudragit S-100 matrix: a synergistic strategy for enhanced oral delivery. Futur Sci OA. 2021;7.
52. Ding Y, Dou C, Chang S, Xie Z, Yu DG, Liu Y, et al. Core-shell eudragit S100 nanofibers prepared via triaxial electrospinning to provide a colon-targeted extended drug release. Polymers (Basel). 2020;12.
53. El-Sheikh SM, Barhoum A, El-Sherbiny S, Morsy F, El-Midany AAH, Rahier H. Preparation of superhydrophobic nanocalcite crystals using Box–Behnken design. Arab J Chem [Internet]. 2019;12:1479–86. Available from: https://doi.org/10.1016/j.arabjc.2014.11.003
54. Sarmento B, Ferreira D, Veiga F, Ribeiro A. Characterization of insulin-loaded alginate nanoparticles produced by ionotropic pre-gelation through DSC and FTIR studies. Carbohydr Polym. 2006;66:1–7.
55. Siddaramaiah, Swamy TMM, Ramaraj B, Lee JH. Sodium alginate and its blends with starch: thermal and morphological properties. J Appl Polym Sci. 2008;109:4075–81.
56. Chawla A, Sharma P, Pawar P. Eudragit S-100 coated sodium alginate microspheres of naproxen sodium: formulation, optimization and in vitro evaluation. Acta Pharm. 2012;62:529–45.
57. Soares JP, Santos JE, Chierice GO, G Cavalheiro ET. Thermal behavior of alginic acid and its sodium salt [Internet]. 2004. Available from: http://www.scielo.br/eq
58. El-Houssiny AS, Ward AA, Mostafa DM, Abd-El-Messieh SL, Abdel-Nour KN, Darwish MM, et al. Drug-polymer interaction between glucosamine sulfate and alginate nanoparticles: FTIR, DSC and dielectric spectroscopy studies. Adv Nat Sci Nanosci Nanotechnol. 2016;7.
59. Nunes R, Bogas S, Faria MJ, Gonçalves H, Lúcio M, Viseu T, et al. Electrospun fibers for vaginal administration of tenofovir disoproxil fumarate and 1 emtricitabine in the context of topical pre-exposure prophylaxis. Available from: https://doi.org/10.1101/2021.02.01.429162
60. Jat R, Jain S, Singh SK, Gupta R. Formulation and in vitro-in vivo evaluation of quercetin loaded Eudragit S100 microspheres. Asian J. Pharm.
61. Politi FAS, Carvalho SG, Rodero CF, dos Santos KP, Meneguin AB, Sorrechia R, et al. Piperine-loaded nanoparticles incorporated into hyaluronic acid/sodium alginate-based membranes for the treatment of inflammatory skin diseases. Int J Biol Macromol. 2023;227:736–48.
62. Schafroth N, Arpagaus C, Jadhav UY, Makne S, Douroumis D. Nano and microparticle engineering of water insoluble drugs using a novel spray-drying process. Colloids Surfaces B Biointerfaces. 2012;90:8–15.
63. Ngema LM, Adeyemi SA, Marimuthu T, Ubanako P, Wamwangi D, Choonara YE. Synthesis of novel conjugated linoleic acid (CLA)-coated superparamagnetic iron oxide nanoparticles (SPIONs) for the delivery of paclitaxel with enhanced in vitro antiproliferative activity on A549 lung cancer cells. Pharmaceutics. 2022;14.
64. Shen Shihoong, Wu Youshen LY and WD. High drug-loading nanomedicines : progress, current status, and prospects. 2017;4085–109.
65. Huda A, Lim KW, Jayanthi B, Palsan SA, Huda MASN, Leony TYS, et al. Optimization of Rhodamine 6G removal from aqueous solution using Box-Behnken design. AIP Conf Proc. American Institute of Physics Inc.; 2021.
66. Bazdaric K, Sverko D, Salaric I, Martinović A, Lucijanic M. The ABC of linear regression analysis: what every author and editor should know. Eur Sci Ed. 2021;47.
67. Benouis K, Alami A, Khalfi Y, Guella S, Khane Y. Optimization of coagulation parameters for turbidity removal using Box-Behnken model. Proc 2nd Int Conf Ind 40 Artif Intell (ICIAI 2021). Atlantis Press; 2022.
68. Sivakumar D. Application of Box Behnken design to optimize the parameters for turning Inconel 718 using coated carbide tools [Internet]. 2013. Available from: http://www.ijser.org
69. Pathak A, Khandegar V, Kumar A. Statistical investigation in conjunction with a Box–Behnken design for the removal of dyes using electrocoagulation. J Hazardous, Toxic, Radioact Waste. 2022;26.
70. Human C, De Beer D, Bowles S, Joubert E. Effect of electrospraying conditions on the properties of aspalathin-Eudragit S100 nanoparticles and assessment of orogastrointestinal stability and membrane permeability. Food Front. 2022;3:285–99.
71. Zhang S, Wang C. Effect of stirring speed on particle dispersion in silica synthesis. Nano-Structures and Nano-Objects. 2023;35:100994.
72. Meng J, Agrahari V, Ezoulin MJ, Purohit SS, Zhang T, Molteni A, et al. Spray-dried thiolated chitosan-coated sodium alginate multilayer microparticles for vaginal HIV microbicide delivery. AAPS J. 2017;19:692–702.
73. Zhang T, Zhang C, Agrahari V, Murowchick JB, Oyler NA, Youan BBC. Spray drying tenofovir loaded mucoadhesive and pH-sensitive microspheres intended for HIV prevention. Antiviral Res. 2013;97:334–46.

Publisher's Note Springer Nature remains neutral with regard to jurisdictional claims in published maps and institutional affiliations.